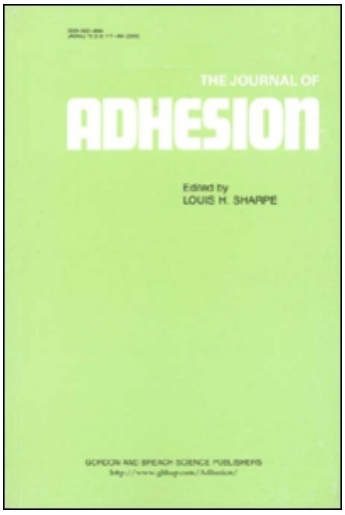

The Journal of Adhesion

Publication details, including instructions for authors and subscription information:
http://www.informaworld.com/smpp/title~content=t713453635

Analysis of the Notched Coating Adhesion Test

David A. Dillard[a]; Buo Chen[a]; Tsunou Chang[ab]; Yeh-Hung Lai[ac]
[a] Engineering Science and Mechanics Department, Virginia Polytechnic Institute and State University, Blacksburg, Virginia, USA [b] Graco, Plymouth, MI, USA [c] Eastman Kodak Company, Rochester, NY, USA

To cite this Article Dillard, David A. , Chen, Buo , Chang, Tsunou and Lai, Yeh-Hung(1999) 'Analysis of the Notched Coating Adhesion Test', The Journal of Adhesion, 69: 1, 99 — 120
To link to this Article: DOI: 10.1080/00218469908015921
URL: http://dx.doi.org/10.1080/00218469908015921

J. Adhesion, 1999, Vol. 69, pp. 99–120
Reprints available directly from the publisher
Photocopying permitted by license only

Analysis of the Notched Coating Adhesion Test *

DAVID A. DILLARD[†], BUO CHEN, TSUNOU CHANG[‡] and YEH-HUNG LAI[¶]

Engineering Science and Mechanics Department, Virginia Polytechnic Institute and State University, Blacksburg, Virginia 24061, USA

(Received 14 October 1997; In final form 18 June 1998)

An analysis of the notched coating adhesion (NCA) test is presented. This simple adhesion test method is appropriate for measuring the interfacial fracture toughness of some classes of coatings and open-faced adhesive bonds. The NCA specimen consists of a single substrate coated with a thin layer of adhesive. The coating is notched to sever the coating and induce sharp interfacial debonds, and the specimen is then loaded in tension. The substrate strain at which coating debonding occurs is recorded and used to determine the critical strain energy release rate. Yielding of the substrate is permitted, and does not significantly affect the calculation of the strain energy release rate. Analytical and finite element analysis are used to quantify the available strain energy release rate for both steady state and laterally-constrained cases. The available strain energy release rate is shown to be quite insensitive to the initial debond length. The specimen geometry results in a mode mix which causes the adhesive to debond along the interface.

Keywords: Notched coating adhesion test; interfacial debond; durability; adhesives; coatings; fracture mechanics

INTRODUCTION

In spite of some progress is predicting adhesive bond and coating performance from constituent properties, determination of bond

* Presented in part at the Nineteenth Annual Meeting of the Adhesion Society, Inc., Myrtle Beach, South Carolina, USA, February 18–21, 1996.

[†] Corresponding author. Tel.: 540-231-4714, Fax: 540-231-9187, e-mail: dillard@vt.edu
[‡] Current address: Graco, 47700 Halyard Drive, Plymouth, MI 48170-2412, USA.
[¶] Current address: Eastman Kodak Company, MC24333, 4/23/KP, Rochester, NY 14652-4333, USA.

properties and durability remains largely an empirical endeavor. Many questions of industrial importance are, at the present time, answered by direct experimental means. Many adhesive producers and users find themselves overwhelmed with the varieties of test methods and number of samples which must be tested, analyzed, and archived. Even relatively minor changes in a product, such as altering the filler content, optimizing the cure process, or modifying the surface pretreatment, may require both short term and long term tests to identify the effects. Unfortunately, many experiments are time consuming to conduct and/or analyze. The widely used single lap joint (SLJ), for example, is easy to fabricate and test, but is complicated to analyze, a fact underscored by the dozens of published papers which purportedly model this specimen. While single lap test results can be useful for quality control and for evaluating the effectiveness of some changes in the material systems, the dependence of the stresses on constituent properties makes direct comparisons of failure stresses difficult. As has been recognized for many years in the mechanics community, and now cautioned by ASTM [1], use of this specimen to obtain design information is problematic. Fracture specimens often require more effort to test, although the critical fracture parameters of the material system in some bonds (*e.g.*, double cantilever beam specimens) can be readily determined. Strength and fracture toughness approaches to design are both utilized, and each approach has its proponents and critics.

One problem associated with typical specimens used to quantify adhesion strength or toughness is the length of time which may be required for moisture to equilibrate within the specimen. Moisture is widely associated with adhesive bond degradation and yet the diffusion properties of most structural adhesives are such that typical specimens may require several years to saturate. Recognizing this limitation, Chang *et al.* [2] proposed utilizing the adhesive as a coating bonded to one substrate rather than as an adhesive sandwiched between two adherends. Rather than diffusing through half the width of a specimen (6–12 mm diffusion path is typical), the moisture only needed to diffuse through the coating thickness (typically less than 1 mm). Since time to reach equilibrium is proportional to the square of the length of the diffusion path, the resulting acceleration can be several orders of magnitude. Furthermore, this acceleration is

accomplished geometrically rather than thermally.[1] This original work also proposed the notched coating adhesion (NCA) specimen which is analyzed herein. A companion paper [3] discusses the practical aspects of utilizing this test method. Several other investigators have subsequently adopted the use of this coating approach to accelerate humidity conditioning, but have then bonded a second adherend onto the conditioned adhesive layer prior to testing. Wylde and Spelt have bonded a relatively thick second adherend to the coating and tested the specimen as a double cantilever beam [4]. They also have apparently coined an apt name for the coating exposure specimen, calling it an "open-faced adhesive" specimen. Jackson *et al.* [5] and Moidu [6] have bonded thinner adherends and then performed testing as 90° peel specimens. All of these works have shown promise for the open-faced specimen to accelerate moisture saturation. Disadvantages of these latter approaches include the time required to form the additional bond between the second substrate and the wet coating surface, and concerns about the integrity of the secondary bond. These problems are avoided with the NCA specimen, but other problems associated with the need to characterize accurately the residual stress and constitutive properties of the coating are present, along with the inherent difficulties in testing coating adhesion.

Test methods for coating adhesion have traditionally been quite problematic, owing primarily to the difficulty in testing the relatively thin coatings with their limited load carrying capabilities. A number of specimens have been proposed and used, as has been reviewed by Chapman *et al.* [7]. These may be categorized into three basic classes. Indirect tests such as the scratch test provide qualitative information about the coating adhesion by measuring the force required to scrape off a section of the coating with a stylus of prescribed shape. Indentation tests could also be placed in this category, although some progress has been made in obtaining quantitative information from such tests [8]. A second category of coating tests involves bonding a second substrate to the coating and then pulling the two adherends apart in tension, torsion, peel, or shear [7]. Depending on the specimen geometry, either strength or fracture toughness values can be obtained

[1] Conditioning at elevated temperature is a common practice to accelerate diffusion, but can lead to spurious degradation modes because of multiple processes with different activation energies.

by these methods provided the secondary bond is better than the coating/substrate adhesion. This is not always the case for high-performance coatings. The third category of tests may be used when the coating has sufficient thickness and toughness to be directly pulled from the substrate. Centrifuge, impact, and ultrasonic techniques have been used in attempts to measure bond strengths. Blister tests of various forms, peel tests, and self-delamination tests have all been used to obtain fracture properties of the bonds.

Dannenberg [9] first proposed the blister test for measuring the adhesion of epoxy coatings. Modifications of the blister test especially suited to coatings include the constrained blister [10], the island blister [11], the peninsula blister [12], and the inverted blister [13]. Depending on the thickness and strength of the coating, as well as the adhesion toughness, a variety of peel tests are also possible. Gripping the coating successfully is a problem with conducting peel tests. Self-delamination tests are especially attractive because they do not require the introduction of mechanically-applied loads to the coating. These tests involve debonding driven by the residual stresses which are commonly induced in the coating due to thermal expansion mismatch. For a biaxial residual stress of σ_0 debonding is predicted when the thickness of the coating exceeds the critical thickness, h_c, as given in:

$$G_c = h_c \sigma_0^2 \frac{1-\nu}{E} \tag{1}$$

where G_c is the critical strain energy release rate of the bond, ν is the Poisson's ratio of the coating, and E is the modulus of elasticity of the coating. To evaluate coating adhesion, one can make specimens with varying thicknesses; those with a thickness exceeding h_c will debond and those less than h_c will not. This provides a means to estimate the critical strain energy release rate. Farris and Bauer [14] and Jensen *et al.* [15] have cut holes or slits in coatings having a thickness greater than h_c. This limits the debonding which occurs, allowing them to quantify G_c with a specimen having a single coating thickness. Film fracture and debonding has been the subject of considerable research, including that of Hu *et al.* [16]; Evans *et al.* [17] and Hu and Evans [18].

Although these self-delamination tests work well with sufficiently thick coatings, there are many cases in which the small coating

thickness and high bond toughness prevent debonding. One method to increase the residual stress is to strain the specimen mechanically. Several authors have loaded specimens containing a brittle coating. The coating cracks, and debonding may emanate from the cracks, allowing estimates of strength and toughness parameters [19]. Cropper and Young [20] notched three-layer polymer–metal laminates and loaded them axially to induce debonding, subtracting the expected plastic work from the total work in order to estimate the debonding energy. The NCA specimen is an extension of these works, but with several differences. A notch is intentionally induced in the coating, thus eliminating the need for testing brittle coatings. Furthermore, the notch is created in such a way that sharp-tipped debonds are initiated at the interface, resulting in a fracture test. This paper will provide an analysis of the technique.

THE NOTCHED COATING ADHESION TEST

The notched coating adhesion (NCA) specimen consists of a thin layer of adhesive bonded to a single substrate as illustrated in Figure 1. A notch is introduced into the adhesive layer near the center of the specimen, severing the coating. This notch may be made by several methods, although the authors have found that "tapping" the notch into the coating by using a utility knife blade and small hammer is

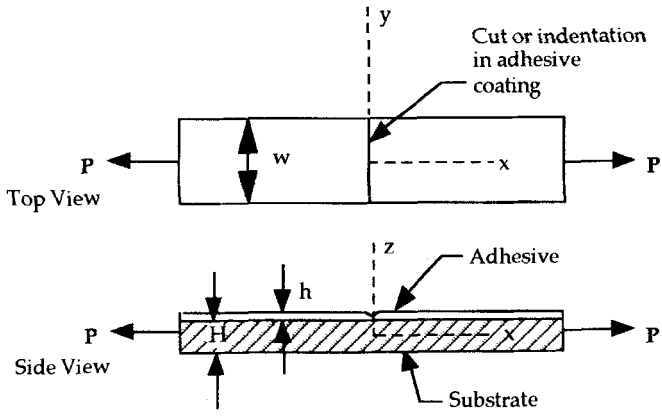

FIGURE 1 The notched coating adhesion specimen.

often appropriate. This notching process places significant stress on the interface, usually producing sharp-tipped cracks propagating along the interface in a fashion similar to that observed by Ritter and his colleagues [21]. These initial debonds, illustrated in Figure 2, are critical to the accuracy of the NCA specimen as they allow it to be analyzed in a fracture mechanics sense. Using an axial loading device, the specimen is then loaded in tension perpendicular to the notch as shown in Figure 1. Axial strain in the substrate is measured using an extensometer. The stress state generated causes the debonds to propagate. This specimen being a constant strain energy release rate specimen, debond propagation does not alleviate the applied strain energy release rate, and the resulting debonding tends to be catastrophic and can be easily observed visually. The critical strain at which the debond starts to propagate is recorded. The critical strain energy release rate can then be determined from the critical strain. In many ways, an NCA specimen is like two cracked lap shear (CLS) specimens attached end to end as can be seen in Figure 3. The mode mixity of the NCA specimen is also similar to the CLS specimen, and may approximate the mode mixes often seen in real bonded structures.

ANALYTICAL ANALYSIS OF THE NCA SPECIMEN

In order to determine the available strain energy release rate for the NCA specimen, we will assume that the coating is relatively thin compared with the substrate, and that the isotropic coating will act in

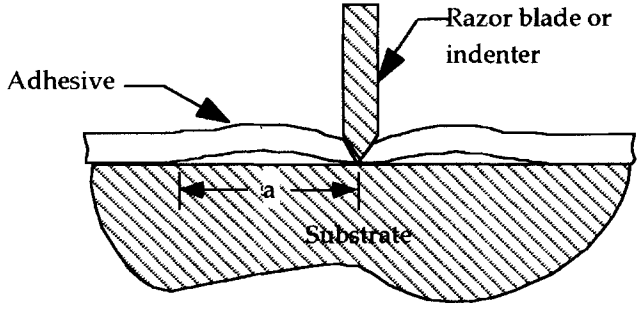

FIGURE 2 Severing the coating and introducing initial debonds with a sharp instrument.

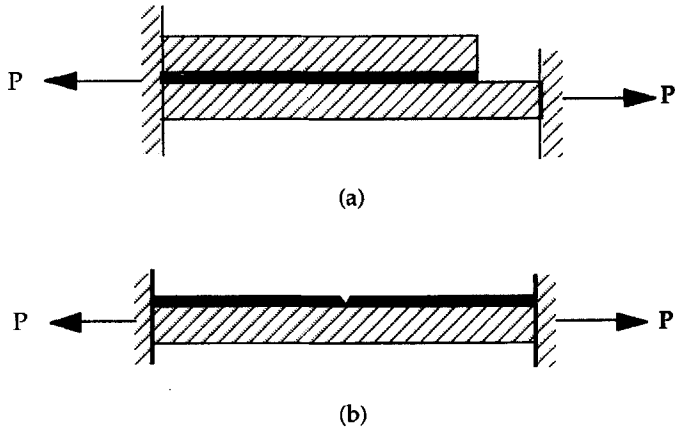

FIGURE 3 A comparison of related specimens: (a) a cracked lap shear specimen (CLS), (b) a notched coating adhesive specimen (NCA).

a linear elastic fashion. A linear elastic assumption will also be made for the substrate, but this will be relaxed later in the paper. The thin nature of the coating will further permit us to ignore bending issues which are of significant importance in the CLS specimens where the lap and strap are often similar in thickness and stiffness [22].

The available strain energy release rate may easily be determined by evaluating the energy stored in a unit area of coating away from the edges or precrack. Here, σ_z, τ_{xz}, and τ_{yz} are zero, and we may write expressions for the in-plane stresses in the coating in terms of the in-plane strains as:

$$\begin{aligned} \sigma_x &= \frac{E}{(1-\nu^2)}(\varepsilon_x + \nu\varepsilon_y) \\ \sigma_y &= \frac{E}{(1-\nu^2)}(\varepsilon_y + \nu\varepsilon_x) \end{aligned} \tag{2}$$

where E and ν are the modulus and Poisson's ratio, respectively, of the coating, and the coordinate system is illustrated in Figure 1. An equal biaxial residual stress is present in the coating which is related to the equal, biaxial residual strain by:

$$\sigma_0 = \frac{E}{(1-\nu)}\varepsilon_0 \tag{3}$$

Residual stresses may result from processing the coating at elevated temperature, through sorption of moisture or other diluents, or through evaporation of solvent in solvent-cast specimens [23], and can also be affected by any curvature of the bonded specimen. This latter source is beyond the scope of the current paper, and residual stresses from all other sources will be combined into a single term as indicated above.

The NCA specimen is loaded axially in the x direction in order to induce debonding. Since the substrate is considered to be massive compared with the coating, the in-plane coating strains will be identical to those of the substrate. At a given mechanically-induced, axial strain, $\hat{\varepsilon}$, the strains in the coating may be expressed as:

$$\begin{aligned} \varepsilon_x &= \varepsilon_0 + \hat{\varepsilon} \\ \varepsilon_y &= \varepsilon_0 - \nu_s \hat{\varepsilon} \end{aligned} \tag{4}$$

where ν_s is the Poisson's ratio of the substrate.

Combining the above equations, we obtain that

$$\begin{aligned} \sigma_x &= \frac{E}{(1-\nu)}\varepsilon_0 + \frac{E}{(1-\nu^2)}(1-\nu\nu_s)\hat{\varepsilon} \\ \sigma_y &= \frac{E}{(1-\nu)}\varepsilon_0 + \frac{E}{(1-\nu^2)}(\nu-\nu_s)\hat{\varepsilon} \end{aligned} \tag{5}$$

The strain energy density in the coating is now given by:

$$u = \frac{1}{2}\left[\sigma_x \varepsilon_x + \sigma_y \varepsilon_y\right] \tag{6}$$

For cases in which the coating is relatively thin and soft compared with the substrate, it can be shown that the change in strain energy which drives the debonding under fixed grip conditions comes almost exclusively from the coating [24]. The following relationships for the available strain energy release rate are derived based on this assumption. When the biaxially-stretched film is debonded along a straight debond front, the available strain energy release rate is easily shown to be:

$$G_{ss} = \frac{hE}{(1-\nu)}\left[\varepsilon_0^2 + \varepsilon_0\hat{\varepsilon}(1-\nu_s) + \frac{\hat{\varepsilon}^2(1-2\nu\nu_s+\nu_s^2)}{2(1+\nu)}\right] \tag{7}$$

for relatively long debonds ($\sigma_y = 0$ within debonded portion.). The "*ss*" subscript indicates that this is the steady-state solution which is appropriate when both a/h and a/w are sufficiently large. (a, h, and w are illustrated in Figs. 1 and 2.) For very short debonds where a/h is less than about five, the equations derived herein are not appropriate, although, as will be shown in the following section, the errors are still quite small. For moderately short debonds in which a/h is on the order of five or more but a/w remains small, lateral constraint prevents the free lateral expansion (due to Poisson's effect) of the debonded coating. Under these short debond conditions, one must subtract the residual energy associated with the debonded coating having a lateral strain as given by Eq. (4):

$$G_{lc} = \frac{hE}{(1-\nu)}\left[\varepsilon_0^2 + \varepsilon_0\hat{\varepsilon}(1-\nu_s) + \frac{\hat{\varepsilon}^2(1-2\nu\nu_s+\nu_s^2)}{2(1+\nu)}\right] - \frac{hE}{2}(\varepsilon_0 - \hat{\varepsilon}\nu_s)^2$$

where the "*lc*" subscript indicates that the debonded coating is laterally constrained to match the lateral strain of the underlying substrate. This in turn simplifies to:

$$G_{lc} = \frac{hE}{2(1-\nu^2)}\left[\varepsilon_0(1+\nu) + \hat{\varepsilon}(1-\nu\nu_s)\right]^2 \tag{8}$$

This distinction between short (laterally-constrained) and long (steady-state) debond lengths will be carried throughout the paper. Terms such as generalized plane strain and plane stress, respectively, could also convey the same idea, but can introduce confusion since the lateral stress or strain constraint actually depends on location along the specimen. In practice, typical initial debond lengths probably result in energy release rates which are intermediate between the short and long debond cases, although the difference is slight as shown in Figure 4.[2] We normally assume the long debond case when making our calculations.

The equations may be simplified if one assumes that the Poisson's ratios of the coating and substrate are equal. For the elastic portion of

[2] For this and several following graphs, the strain energy release rate is nondimensionalized by dividing by the coating thickness and modulus.

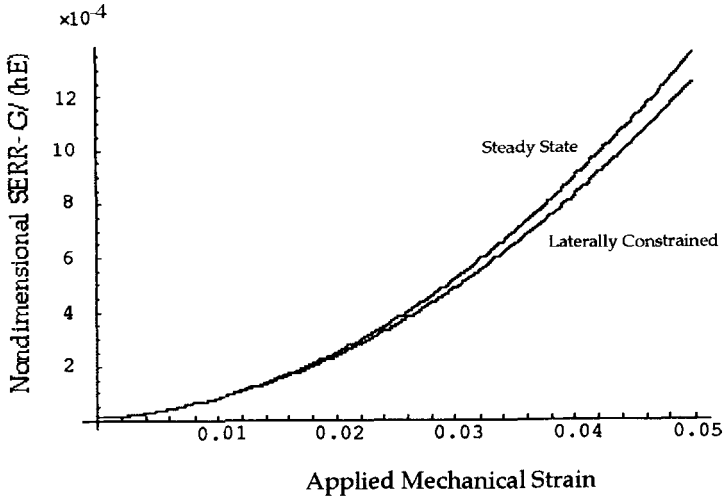

FIGURE 4 A comparison of steady state and laterally constrained nondimensional strain energy release rates (SERR) for a residual strain of 0.2% ($\nu = \nu_s = 1/3$).

the deformation, the Poisson's ratio of a typical metal adherend may be slightly smaller that of a typical polymer coating. Once yielding of the substrate occurs, however, the effective Poisson's ratio for the yielded member approaches a value of 0.5. The simplified forms assuming that the Poisson's ratios are the same are given by:

$$G_{ss} = hE\left[\frac{\varepsilon_0^2}{(1-\nu)} + \varepsilon_0\hat{\varepsilon} + \frac{\hat{\varepsilon}^2}{2}\right] \tag{9}$$

for steady state debonding, and for laterally-constrained debonds:

$$G_{lc} = hE\frac{(1+\nu)}{2(1-\nu)}\left[\varepsilon_0 - \nu\hat{\varepsilon} + \hat{\varepsilon}\right]^2 \tag{10}$$

The corresponding forms in terms of the residual stress are:

$$G_{ss} = \frac{h}{E}\left[(\sigma_0^2 + \sigma_0\hat{\varepsilon}E)(1-\nu) + \frac{\hat{\varepsilon}^2E^2}{2}\right] \tag{11}$$

which was previously reported for steady-state [25], and for laterally-constrained debonds:

$$G_{lc} = \frac{h}{2E}(1-\nu^2)(\sigma_0 + \hat{\varepsilon}E)^2 \tag{12}$$

A graph of the steady-state case reveals that for a polymer with a Poisson's ratio of 0.333, changing the Poisson's ratio of the substrate from 0.25 to 0.5 does not result in any significant difference in the strain energy release rate. For the short debond case, there is some difference as shown in Figure 5.

The residual stress can play a significant role in the magnitudes of the available strain energy release rate. Figure 6 illustrates this effect for several positive values of residual strain.[3] For the case of no residual stress, simple relations may be given for the ratio of the steady-state value to the laterally constrained value: $(1 - 2\nu\nu_s + \nu_s^2)/(1 - \nu\nu_s)^2$ or $1/(1-\nu^2)$ for the case where the two Poisson's ratios are equal. When the residual stress is not equal to zero, the ratio of the steady-state to laterally-constrained results is a function of the applied mechanical strain. The ratio of the steady-state to laterally-constrained values for the case where Poisson's ratio is 0.333 for both the coating and substrate is plotted in Figure 7 for several values of residual strain.

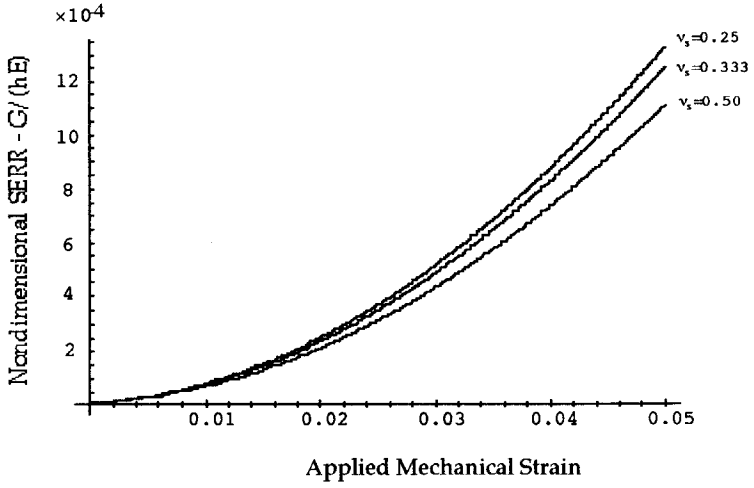

FIGURE 5 Nondimensional strain energy release rate (laterally constrained) as a function of applied mechanical strain for a residual strain of 0.2%. $\nu = 1/3$, $\nu_s = \{0.25, 1/3, 0.5\}$.

[3] Because polymeric coatings are often processed at higher temperatures than their service temperatures, residual strains are normally tensile, although this is not always the case.

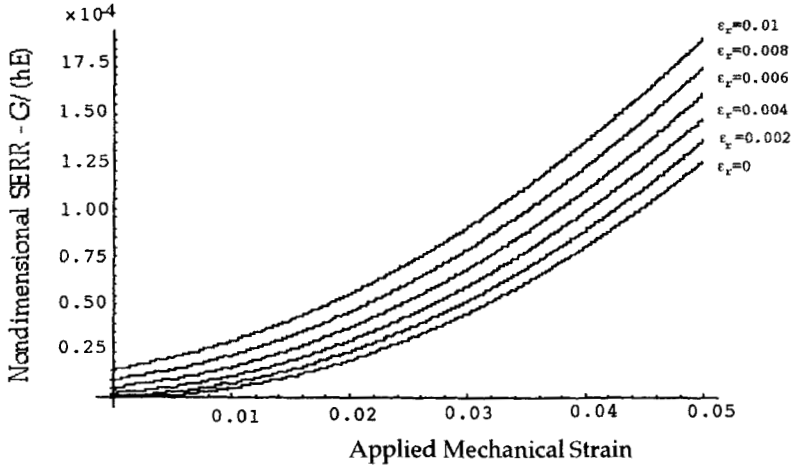

FIGURE 6 Nondimensional applied strain energy release rate (steady state) as a function of applied mechanical strain for various values of residual strain ($\nu = \nu_s = 1/3$).

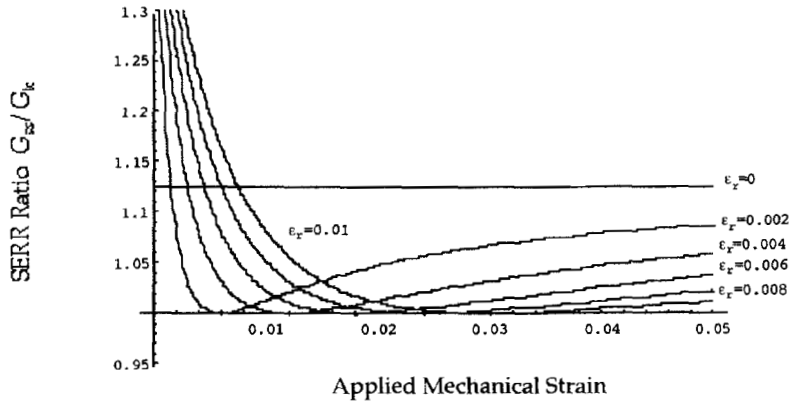

FIGURE 7 Ratio of steady state to laterally constrained values of the strain energy release rate as a function of applied mechanical strain for various values of residual stress ($\nu = \nu_s = 1/3$).

It is interesting to note that for each value of residual strain, there is a value of applied strain at which the steady state and laterally constrained energy release rates are equal.

FINITE ELEMENT ANALYSIS OF THE NCA SPECIMEN

A geometrically-nonlinear finite element analysis of a typical (epoxy on steel) NCA geometry was conducted using ABAQUS [26] in order to evaluate the accuracy of the analytical expressions. Eight node, plane stress, CPS8R elements were used with reduced integration. Singular elements were used around the debond tip. The steel substrate was modeled as an elastic-perfectly plastic material (E_s = 203 GPa, ν_s = 0.33, σ_y = 200 MPa) and the epoxy coating was modeled as an elastic material (E = 2.97 GPa, ν = 0.33). The coating and substrate were 0.15 and 2 mm thick, respectively. For this system, the (plane stress) Dundur's parameter [27], $\alpha = (E-E_s)/(E + E_s)$, was −0.971. The J-integral was calculated around five contour lines (four of which are shown in Fig. 8). The deviation of the J-integral for the outer three contours were always within 1%, indicating good consistency. Good agreement was seen between the plane stress finite element results and the closed-form solution as illustrated in Figure 9.

The distinction between plane stress and plane strain designations used in the finite element model and the steady-state and laterally-

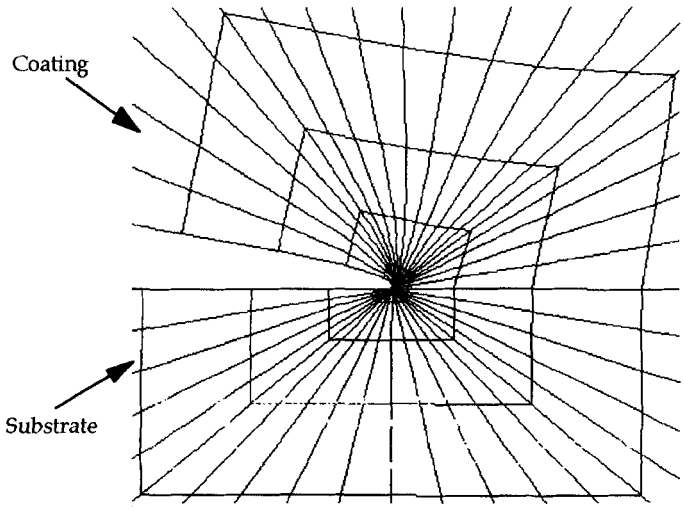

FIGURE 8 Finite element mesh around the deformed crack tip at a magnification ratio of 4.4 for a = 5 mm. The four contours represent some of the J-integral contours examined.

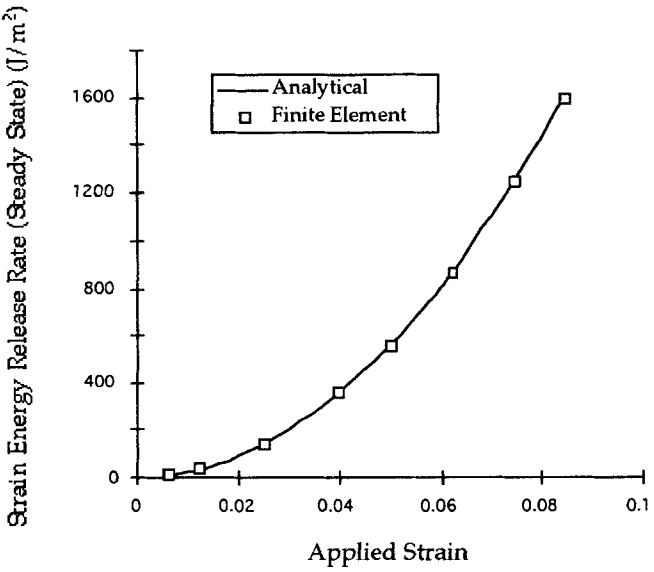

FIGURE 9 Strain energy release rate *versus* applied strain for both finite element (plane stress) and analytical (steady state) solutions for the case of no residual stress and $a = 5$ mm.

constrained analytical solutions became apparent when modeling and comparing solutions. The actual NCA geometry is, of course, a 3-D problem, so plane stress and plane strain representations are somewhat crude. Altering Poisson's ratios can improve the correspondence between actual geometry, analytical solutions, and numerical approximations, providing more meaningful evaluations of the accuracy of the closed-form solutions. These comparisons were made using the moduli and thickness as stated earlier, and again using $\varepsilon_0 = 0$ and $\hat{\varepsilon} = 2.5\%$. By making $\nu_s = 0$, lateral strains are zero, so should correspond with both the steady-state and laterally-constrained case, as shown in Table I. Making $\nu_s = \nu$ allows meaningful plane stress analysis, again accurately approaching the steady-state solutions for our example problem. Table I shows the excellent agreement.

The analytical relationships all assume that the debond is propagating in a self-similar manner with a straight debond front. This requires that the initial debond be several times longer than the coating thickness in order to have self-similar propagation. The

TABLE I Improved correspondence between actual geometry, analytical solutions, and FEA results by altering Poisson's ratio

Case Studied	ν_s	ν	J_{FEAS} (J/m^2)	G_{ss} (J/m^2)	G_{lc} (J/m^2)	*% error*
Plane Strain FEA	0	0.33	154.1	156.2	156.2	1.3
Plane Strain FEA	0	0	137.5	139.2	139.2	1.2
Plane Stress FEA	0	0	137.5	139.2	139.2	1.2
Plane Stress FEA	0.33	0.33	138	139.2	124.0	0.8(ss)

creation of these initial debonds is an important feature of the NCA specimen, allowing debonds to grow from sharp-tipped cracks with a square root singularity. Tapping the debonds into the specimen in the manner described above gives limited control over the length of these initial flaws. The debond length of the finite element model was varied to determine the sensitivity of the strain energy release rate to the initial debond length. The highly-expanded scale in Figure 10 shows that an initial debond of at least $a = 10h$ is ideal. Similar results have been reported, for example, by Ye *et al.* [28] for similar values of Dundur's α.

The analytical expressions for G neglect the behavior of the substrates by assuming a relatively thin, flexible coating on a massive and stiff substrate. Although not explicitly stated, this in effect allows the

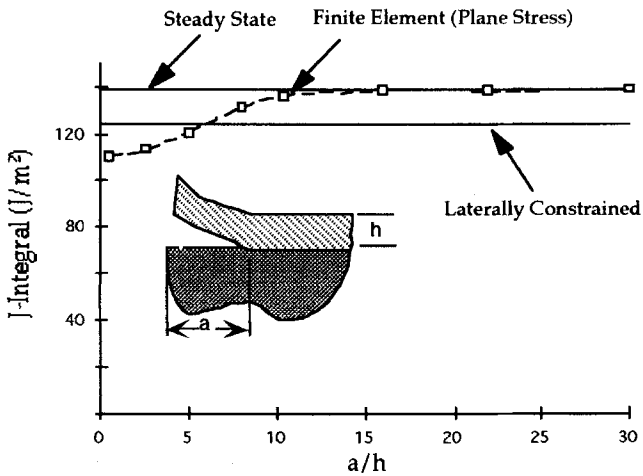

FIGURE 10 Applied strain energy release rate (G) *versus* nondimensional initial debond length for the case of Dundurs' $\alpha = -0.9$.

substrates to yield without significantly affecting the results. In an effort to verify this assumption, the yield stress of the steel substrate in the finite element model was varied, effectively resulting in more or less plastic flow at any given mechanical strain. The J-integral was determined for the various runs, and these values are shown in Figure 11. Again, the highly-magnified axis indicates that the entire range of plastic strain considered results in only very minor changes in the J-integral values obtained. This confirms that substrate yielding is permitted with the NCA specimen, and does not substantially affect the analytical predictions, provided the other assumptions remain valid.

Finally, as has been noted earlier, the NCA specimen differs from prior work which focused on relatively stiff coatings bonded on softer substrates. The NCA analysis is not directly applicable to such cases, although approximate corrections can be made to the analytical expressions for strain energy release rate by multiplying them by the factor $[1 + (hE)/(HE_s)]$, the term which comes out of the cracked lap shear (CLS) analysis [29]. With this correction factor applied, the

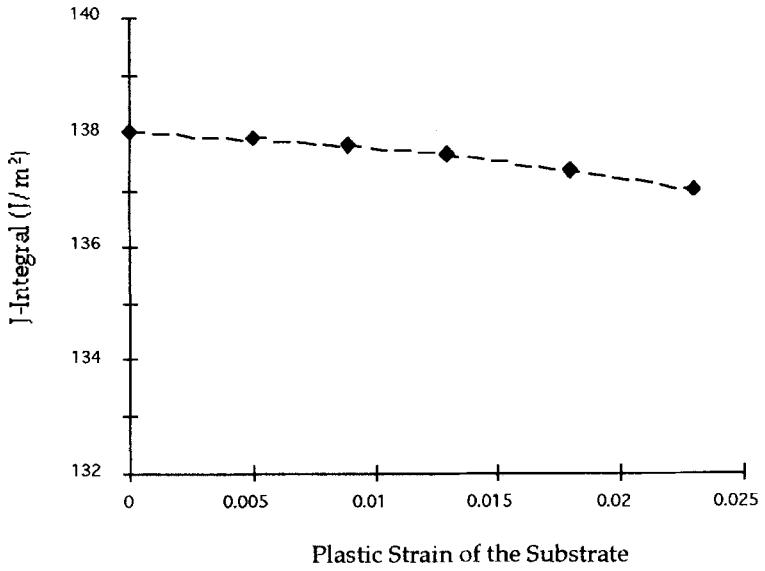

FIGURE 11 J-integral for NCA specimen in which the plastic strain in the substrate is varied at a fixed value of mechanical strain.

simple analysis correlates well with the finite element (plane stress) results where α is allowed to range from -1 to 1 by changing the moduli of the substrate and coating. Figure 12 shows that the agreement is quite good for values of α ranging from -1 (typical of polymer coatings on the metal substrates) to 1 (typical of metal or ceramic coatings on polymer substrates).

MODE MIXITY AND FRACTURE EFFICIENCY

The strain energy release rate that causes the debond to propagate is referred to as the "critical strain energy release rate". The NCA specimen can be modeled as a layered bi-material where the adhesive is a very thin layer on top of a thick substrate. To determine the contribution from each mode to the strain energy release rate obtained, Suo and Hutchinson's layered bi-material analysis [30] is applied. If the adhesive is much thinner than the substrate, the mode mixity depends only on the angular quantity ω:

$$\frac{G_{II}}{G_I} = \tan(\omega)^2 \tag{13}$$

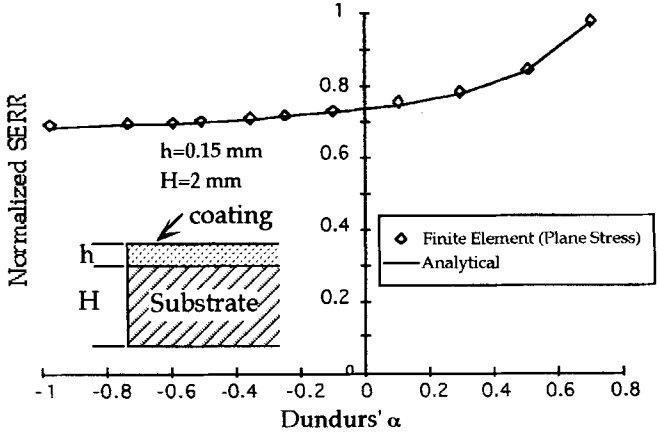

FIGURE 12 Normalized applied strain energy release rate (G) *versus* the Dundurs' parameter α for both finite element and analytical solutions. (For comparison purposes, all values were divided by the highest value obtained).

ω is a function of Dundurs' parameters, α and β, and has been tabulated [30]. For typical adhesive systems, ω ranges from 40° to 70°; the preferred failure direction for this range is directed towards the interphase, just the opposite of many tests. An inherent advantage to this type of mixed-mode fracture test is that there is an incentive for the adhesive to fail near the interface.[4] This may be advantageous when one is attempting to characterize the interface and associated degradation. The specimen is also especially convenient for extracting samples for surface analysis [3].

A comparison of the fracture efficiency parameter of the NCA with other adhesive test methods is also insightful. Lai and Dillard have introduced the concept of the fracture efficiency parameter [31], and have used this concept to compare the efficiency of various coating [32] and adhesion [33] tests. The fracture efficiency parameter is defined by [33]:

$$T_e = \frac{G}{\sigma_{\max}^2} \tag{14}$$

where G is the available strain energy release rate and $\sigma_{\max}$ is the maximum non-singular stress.[5] The fracture efficiency parameter can be used to determine which loading scenario is most likely to induce debonding without yielding or rupturing the coating or adherends. Figure 13 shows a comparison of various fracture test for adhesives with a zero prestress. The 0° peel and NCA specimen both have the highest nondimensional fracture efficiency parameter which is theoretically possible for specimens with non-negative prestress. These high values are possible for the NCA specimen because only yielding of the coating is considered in determining T_e; substrate yielding is permitted and does not significantly affect the results. It is interesting to note that the CLS specimen with a very similar geometry to the NCA specimen has the lowest T_e. This is because the CLS specimen is normally tested in such a way that the lap and strap both behave in an

[4] A number of specimens have been tested to date from a wide variety of material systems; all have visually appeared to be interfacial failures.

[5] Various stress metrics are possible; here we simply use the axial stress induced by the combined action of bending and axial loading of the two adherends, or adherend and coating.

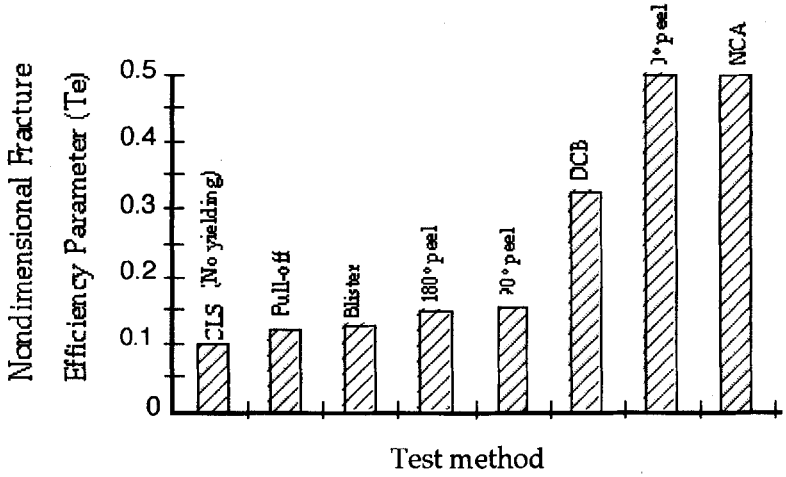

FIGURE 13 Applied strain energy release rate (G) *versus* nondimensional initial debond length for the case of Dundurs' $\alpha = 0.9$.

elastic fashion. Were the strap allowed to yield, as in the NCA specimens, both configurations would have the same T_e. In this form, the fracture efficiency parameter does not reflect mode mix and the fact that the critical energy release rates may vary with mode mixity. Nonetheless, it is seen that the NCA geometry is an attractive specimen where one desires debonding rather than coating failure.

Finally, although the coating has been assumed to behave in a linear elastic fashion for the purposes of the equations derived herein, the NCA geometry can also be applicable to specimens in which the coating exhibits nonlinear behavior. As illustrated in Figure 9 good consistency was observed between the geometrically-nonlinear finite element results and the closed-form solution where the coating was assumed to be linear elastic. For relatively stiff substrates, the energy available to drive the debond comes primarily from the coating. Thus, one only needs to determine the stored elastic energy in the yielded coating to determine the available strain energy release rate. For materials which unload in a linear fashion, this determination is especially easy. In contrast to many test geometries in which adhesive yielding would alter the calculated critical strain energy release rate, the NCA specimen does not appear to be affected, provided yielding is properly included as stated.

SUMMARY AND CONCLUSIONS

Simple closed-form solutions have been obtained for determining the available strain energy release rate of the notched coating adhesion (NCA) test. Key assumptions are that the coating is relatively thin and compliant in comparison with the substrate, that bending is not significant due to the fact that the coating produces little eccentricity, and that although the substrate may yield, the coating remains linear elastic (although use of stored energy can be used if coating yielding occurs). The NCA test has proved to be especially useful for durability studies due to the specimen's greatly reduced time to saturate the bond. The test is also appropriate for interface and surface treatment studies because of its tendency to cause interfacial failure. Although not intended to replace conventional adhesion tests, the method is believed to have significant potential for durability investigations.

This test method offers a quantitative method to characterize the interfacial fracture toughness of coating/substrate adhesion in situations where the coating is sufficiently thick and stiff to supply the necessary energy to the debond front. Adding reinforcement can allow the use of this method in situations where the coating is not thick enough to allow for direct testing with this technique. The specimen is believed to offer the following advantages:

(1) Coating is severed in such a way as to induce sharp-tipped debonds for true fracture mechanics testing
(2) Mechanical loading provides additional driving force to cause debonding in systems where the residual stresses are not sufficient to drive the debond
(3) Accurate analytical expressions are available for determining the strain energy release rate
(4) Yielding of the adherend is permitted, and does not significantly alter the available energy for fracture
(5) Specimen provides a mode mix which may approximate that seen in actual bonded structures
(6) Mode mix forces the crack to propagate along the interface, resulting in an interfacial failure which can readily be analyzed with surface analysis techniques

(7) Specimen has the highest theoretical fracture efficiency of any unreinforced coating fracture test with a non-negative prestress, suggesting high likelihood of debonding rather than coating rupture or yielding in comparison with alternate test methods.
(8) Testing scheme may be used with coating specimens which have been exposed to environmental conditions in an effort to accelerate adhesive conditioning
(9) The NCA specimens appears to be readily adaptable to situations in which the coating may undergo yielding as well.

Possible limitations with the geometry are the need to know accurately the residual stress state and constitutive properties of the coating at the time of testing. Since these properties are often not as well characterized as those of the substrate, special efforts may be required to obtain this information. This could be especially important for materials whose constitutive properties change with environmental exposure.

Acknowledgments

The authors wish to thank the Center for Adhesive and Sealant Science, the Adhesive and Sealant Council, Inc. and the National Science Foundation-Science and Technology Center #DMR-912004 for supporting this research. We also appreciate the help of Dr. Nick Shephard and two undergraduate students: Ms. Elizabeth Sproat and Ms. Holly Gurbacki.

References

[1] ASTM D4896-89: "Use of Adhesive-Bonded Single Lap-Joint Specimen Test Results", *Annual Book of ASTM Standards* **15**(06), 407 (1994).
[2] Chang, T., Lai, Y. H., Shephard, N. E., Sproat, E. A. and Dillard, D. A., *Proceedings of the 18th Annual Meeting of the Adhesion Society*, Holubka, J. W., Ed., p. 108 (1995).
[3] Clark, R. L., Giunta, R. K., Craven, M. D., Chen, B., Kander, R. G. and Dillard, D. A., "Applications of The Notched Coating Adhesion Test", *J. Adhesion* in preparation.
[4] Wylde, J. W. and Spelt, J. W., *Proceedings of the 19th Annual Meeting of the Adhesion Society*, Ward, T. C., Ed., p. 478 (1996).
[5] Jackson, R. S., Kinloch, A. J., Gardhan, L. M. and Bowditch, M. R., *Proceedings of the 19th Annual Meeting of the Adhesion Society*, Ward, T. C., Ed., p. 147 (1996).

[6] Moidu, A. K. "Destructive and Ultrasonic Characterization of Adhesive Joint Durability using Open-facedSpecimens", *Ph. D. Dissertation*, U. of Toronto, 1997.
[7] Chapman, B. A., DeFord, H. D., Wirtz, G. P. and Brown, S. D., *Proceedings of the ASME Winter Annual Meeting: Technology of Glass, or Glass-Ceramic to Metal Sealant*, p. 77 (1988).
[8] Ritter, J. E., Lardner, T. J., Rosenfeld, L. and Lin, M. R., *J. Applied Physics* **66**, 3626 (1989).
[9] Dannenberg, H., *J. Applied Polymer Sci.* **5**, 125 (1961).
[10] Chang, Y. S., Lai, Y. H. and Dillard, D. A., *Adhesion* **27**, 197 (1989).
[11] Allen, M. G. and Senturia, S. D., *J. Adhesion* **29**, 219 (1989).
[12] Dillard, D. A. and Bao, Y., *J. Adhesion* **33**, 253 (1991).
[13] Fernando, M., Kinloch, A. J., Vellerschamp, R. E. and van der Linde, W. B., *J. Materials Science Letters* **12**, 875 (1993).
[14] Farris, R. J. and Bauer, C. L., *J. Adhesion* **26**, 293 (1988).
[15] Jensen, H. M., Hutchinson, J. W. and Kim, K. S., *Int. J. Solids and Structures* **26**, 1099 (1990).
[16] Hu, M. S., Thouless, M. D. and Evans, A. G., *Acta Metall.* **36**, 1301 (1988).
[17] Evans, A. G., Drory, M. D. and Hu, M. S., *J. Mater. Res.* **3**, 1043 (1988).
[18] Hu, M. S. and Evans, A. G. *Acta Metall.* **37**, 917 (1989).
[19] Chow, T. S., In: *Adhesion Science and Technology*, 9B, Lee, L. H., Ed. (Plenum, New York, 1975), p. 687.
[20] Cropper, K. R. and Young, R. J., *J. Adhesion* **34**, 153 (1991).
[21] Lin, M. R., Ritter, J. E., Rosenfeld, L. and Lardner, T. J., *J. Mater. Res.* **5**, 1110 (1990).
[22] Lai, Y. H., Rakestraw, M. D. and Dillard, D. A., *Int. J. Solids and Structures* **33**, 1725 (1996).
[23] Croll, S. G., *J. Appl. Polym. Sci.* **23**, 847 (1979).
[24] Dillard, D. A. "J-Integral Analysis of NCA and CLS Specimens", Manuscript in preparation.
[25] Chang, T., Sproat, E. A., Lai, Y. H., Shephard, N. E. and Dillard, D. A., *J. Adhesion* **60**, 153 (1997).
[26] ABAQUS 5.4 Software, Hibbitt, Karlsson, and Sorensen, Inc. (1994).
[27] Dundurs, J., *J. Appl. Mechanics*, **36**, 650 (1969).
[28] Ye, T., Suo, Z. and Evans, A. G., *Int. J. Solids and Structures* **29**, 2639 (1992).
[29] Brussat, T. R., Chiu, S. T. and Mostovoy, S., *Fracture Mechanis for Structural Adhesive Bonds*, AFML-TR-77-163, Air Force Materials Laboratory, Wright-Patterson AFB, Ohio (1997).
[30] Suo, Z. and Hutchinson, J. W., *Int. J. Fracture* **43**, 1 (1990)
[31] Lai, Y. H. and Dillard, D. A., *J. Adhesion Sci. and Technol.* **8**, 663 (1994).
[32] Lai, Y. H. and Dillard, D. A., *J. Adhesion* **56**, 509 (1996).
[33] Lai, Y. H. and Dillard, D. A., *Int. J. Solids and Structures* **34**, 509 (1997).